



Anomalously high electronic thermal conductivity and Lorenz ratio in Bi_2Te_3 nanoribbons far from the bipolar condition

Cite as: Appl. Phys. Lett. **114**, 152101 (2019); <https://doi.org/10.1063/1.5092221>

Submitted: 08 February 2019 . Accepted: 26 March 2019 . Published Online: 15 April 2019

Hwan Sung Choe, Jiachen Li , Wenjing Zheng, Jaejun Lee, Joonki Suh , Frances I. Allen, Huili Liu, Heon-Jin Choi, Wlodek Walukiewicz, Haimei Zheng, and Junqiao Wu



View Online



Export Citation



CrossMark

Applied Physics Reviews
Now accepting original research

2017 Journal
Impact Factor:
12.894

AIP
Publishing

Anomalously high electronic thermal conductivity and Lorenz ratio in Bi₂Te₃ nanoribbons far from the bipolar condition

Cite as: Appl. Phys. Lett. **114**, 152101 (2019); doi: 10.1063/1.5092221

Submitted: 8 February 2019 · Accepted: 26 March 2019 ·

Published Online: 15 April 2019



View Online



Export Citation



CrossMark

Hwan Sung Choe,^{1,2,a)} Jiachen Li,^{1,3,a)} Wenjing Zheng,^{1,3} Jaejun Lee,⁴ Joonki Suh,^{1,3} Frances I. Allen,^{1,5,6} Huili Liu,^{1,3} Heon-Jin Choi,⁴ Wlodek Walukiewicz,³ Haimei Zheng,^{1,3} and Junqiao Wu^{1,2,3,b)}

AFFILIATIONS

¹Department of Materials Science and Engineering, University of California, Berkeley, California 94720, USA

²Tsinghua Berkeley Shenzhen Institute, University of California, Berkeley, California 94720, USA

³Division of Materials Sciences, Lawrence Berkeley National Laboratory, Berkeley, California 94720, USA

⁴Department of Materials Science and Engineering, Yonsei University, Seoul 03722, Korea

⁵National Center for Electron Microscopy, Molecular Foundry, Lawrence Berkeley National Laboratory, Berkeley, California 94720, USA

⁶California Institute for Quantitative Biosciences, University of California, Berkeley, California 94720, USA

^{a)}Contributions: H. S. Choe and J. Li contributed equally to this work.

^{b)}Author to whom correspondence should be addressed: wuj@berkeley.edu

ABSTRACT

The Lorenz number (L) of a conductor is the ratio between its electronic thermal conductivity and electrical conductivity. It takes the Sommerfeld value of $L_0 = (\pi^2/3)(k_B/e)^2$ in simple, metallic electronic systems where charge and heat are both carried by the same group of quasi-particles that experience elastic scattering. Higher values of L than L_0 are possible in semiconductors where both electrons and holes co-exist at high densities, that is, in bipolar conduction. As a narrow-bandgap semiconductor, Bi₂Te₃ exhibits $L > L_0$ which has been generally attributed to such bipolar conduction mechanisms. However, in this work, we report that $L > L_0$ is still observed in individual, single-crystal Bi₂Te₃ nanoribbons even at low temperatures and when degenerately doped, that is, far from the bipolar conduction condition. This discovery calls for different mechanisms to explain the unconventional electronic thermal transport behavior in Bi₂Te₃.

Published under license by AIP Publishing. <https://doi.org/10.1063/1.5092221>

In conductive materials, thermal conductivity (κ) comprises the contributions from phonons and charge carriers, $\kappa = \kappa_{ph} + \kappa_e$. Although difficult to separate from the phonon contribution (κ_{ph}), the charge carrier contribution (κ_e) is usually proportional to the electrical conductivity (σ) of charge carriers, via a relationship known as the Wiedemann-Franz law, $\kappa_e = L \cdot \sigma T$. Here, T is the absolute temperature and L is the Lorenz ratio. The value of L is dependent on the charge scattering mechanism, the temperature, and the carrier density.^{1,2} At the degenerate doping limit with dominant elastic carrier scattering, L is not much different from the Sommerfeld value $L_0 = (\pi^2/3)(k_B/e)^2 = 2.44 \times 10^{-8} \text{ W}\Omega/\text{K}^2$. Deviation of L from L_0 typically occurs at cryogenic temperatures,^{3–11} and arises due to unconventional phases of matter, strong inelastic scattering of quasi-particles, bipolar conduction,² or non-quasi-particle transport.¹¹

For Bi₂Te₃ in particular, previous reports have provided evidence of $L > L_0$, but all under the bipolar conduction condition.^{12,13} As a narrow-bandgap semiconductor with a bandgap of only $E_G \approx 0.17 \text{ eV}$, free electrons and holes can be easily thermally excited across the bandgap, resulting in the coexistence of a considerable density of both free electrons and holes, even in the case of moderate extrinsic doping. In this case, the Fermi level is near the middle of the bandgap or within the bandgap, exhibiting bipolar transport. In the bipolar transport condition, there are two mechanisms that could lead to $L > L_0$. The first mechanism^{14,15} is a classical effect caused by the uni-directional drift of electrons and holes: electrons and holes are thermally generated in a hot region, and both drift along the temperature gradient. Upon reaching the cold region, they recombine and release energy as heat, thereby transporting more thermal energy than in the case of

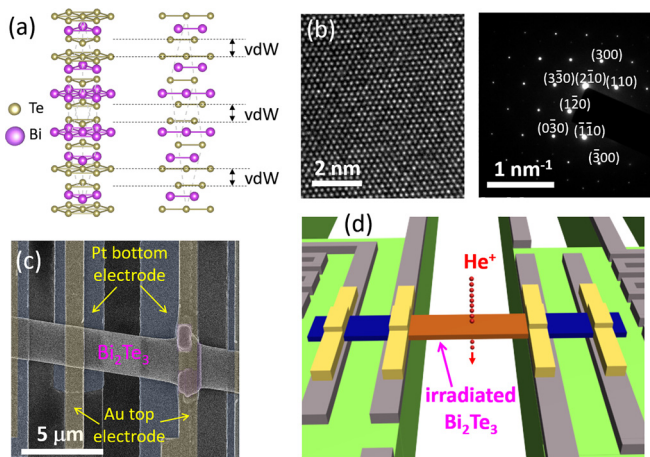


FIG. 1. A single Bi_2Te_3 nanoribbon bridging two pads of a suspended microdevice for simultaneous thermal and electrical measurements. (a) Schematic of the crystal structure of Bi_2Te_3 . (b) (Left) HRTEM lattice image of a pristine Bi_2Te_3 nanoribbon. (Right) The corresponding SAED pattern. (c) SEM image of a suspended microdevice bridged by a Bi_2Te_3 nanoribbon. False colors are used to show the electrodes as indicated. (d) Perspective schematic of helium ion irradiation of the Bi_2Te_3 nanoribbon.

unipolar transport. The second, more exotic mechanism^{10,16} is attributed to the radically different ways in which electron-hole interactions affect the charge and heat flows: under an electrical field, electrons and holes move in opposite directions, hence the collisions between them (viscosity of the electron-hole system) would efficiently reduce the electrical conduction; under a temperature gradient, in contrast, electrons and holes move along the same direction; hence, their thermal conductivity is not affected by the viscosity, and is limited by carrier-impurity scattering instead. This effect is described as hydrodynamic behavior of electrons. In clean hydrodynamic systems when impurity density is low, the Lorenz ratio $L = \kappa_e / \sigma T$ could easily exceed L_0 . Indeed, the values of L up to $20L_0$ have been reported in graphene in the bipolar conduction regime.¹⁰ For Bi_2Te_3 and $\text{Bi}_2\text{Te}_3\text{Se}$ thin flakes, L values of $\sim 2L_0$ ¹³ and $\sim 10L_0$,¹² respectively, have been observed, and were tentatively attributed to either of these bipolar conduction mechanisms, although evidence of bipolar conduction was not presented in those systems.

Both of the above effects originate from bipolar transport, which is not taken into account in derivation of the Sommerfeld value of the Lorenz ratio. In this work, we experimentally determine the upper and lower bounds of L as a function of temperature and charge carrier doping. We discovered that $L > L_0$ for a clearly unipolar, electron conduction condition, which cannot be described by current bipolar transport theories.

The Bi_2Te_3 nanoribbons used in this work were synthesized by a Chemical Vapor Deposition (CVD) process. Bi_2Te_3 powder (Sigma-Aldrich) and silicon substrates were placed at the center and downstream of a tube furnace, respectively. H_2 (3000 sccm) and Ar (300 sccm) gases were used as both the source carrier and the purging gas. The temperature of the furnace was elevated to 520°C for 12 min and maintained for 28 min. Afterwards, the furnace was allowed to cool naturally to room temperature. Most of the data shown here were collected from a Bi_2Te_3 nanoribbon of 62 nm thickness, but

experiments have also been performed on other nanoribbons with different thicknesses, and similar results were observed.

Figure 1(a) shows schematically the layered structure of Bi_2Te_3 , where each quintuple atomic sheet is separated from its neighbors by a van der Waals gap. The as-grown Bi_2Te_3 nanoribbons were evaluated by high-resolution transmission electron microscopy (HRTEM) and selected area electron diffraction (SAED), as shown in Fig. 1(b). These analyses confirm that the nanoribbons are single crystalline, with an atomically clean surface and edges.

In order to study the thermal, electrical, and thermoelectric properties of these nanoribbons, we used suspended micro-pad devices,¹⁷ as shown in Fig. 1(c) and schematically in Fig. 1(d). A single nanoribbon was dry transferred such that it bridged the two SiN_x pads, each of which is suspended from the substrate via long and flexural arms. Pt electrodes were lithographically pre-patterned onto the pads to serve as four-point-probe Pt contacts to the nanoribbon, or as a serpentine heater and a thermometer for thermal measurements.¹¹ To ensure good thermal and electrical contact of the nanoribbon with the underlying Pt electrodes, we also deposited 100-nm-thick Au electrodes onto the Bi_2Te_3 nanoribbon using e-beam lithography, and when needed, further clamped the nanoribbon by selective gallium focused ion beam (FIB) induced deposition of Pt at the edge of the contacting area [Fig. 1(c)]. This approach provides firm and ohmic contacts, yet avoids long exposure of the nanoribbon to the FIB which would cause unwanted damage to the material.

To separate the electronic and phonon contributions to the thermal conductivities, we take advantage of the fact that electrical and lattice thermal conductivities of Bi_2Te_3 respond oppositely to native point defects (atomic vacancies and interstitials). That is, Bi_2Te_3 's lattice thermal conductivity decreases with defect density as expected for crystalline materials, but its electrical conductivity increases with defect density.^{18,19} The latter is mostly due to the rapid rise in free electron density donated by these electrically active point defects, which overpowers the reduction in electron mobility caused by added impurity scattering, as observed for Bi_2Te_3 thin films and explained in Ref. 18. The narrow width of our nanoribbons prevents Hall effect experiments to be performed on the samples; however, electrical transport behavior of Bi_2Te_3 in response to ion irradiation has been well characterized using Hall effect measurements of thin films.¹⁸ We introduced these native point defects into our nanoribbons by irradiating the material with focused, 30 keV He^+ ions using a Zeiss ORION NanoFab Helium Ion Microscope (HIM). This medium-level energy is chosen to find a balance between (a) maximization of nuclear stopping power (favoring low energy) to create lattice defects and (b) maximization of the ion projected range (favoring high energy) to avoid unwanted doping of nanoribbons with He. The Monte Carlo Stopping and Range of Ions in Matter (SRIM) program was used to simulate the generation of point defects by irradiation.²⁰ For 30 keV He^+ ions incident on Bi_2Te_3 , the projected range estimated by SRIM is ~ 148 nm, such that $>99.9\%$ of the ions travel entirely through a nanoribbon of thickness of 62 nm or less, leaving behind only lattice damage and native point defects that are dependent on the irradiation dose. In our experiments, the nanoribbon channel is uniformly irradiated by rastering the He^+ ion beam over the entire suspended region, and the irradiation dose is calculated from the current and rastering parameters implemented. The thermal and electrical measurements were performed under high vacuum ($<1 \times 10^{-7}$ Torr) in a cryostat to avoid convective heat loss.

Figures 2(a)–2(c) show the measured total thermal conductivity (κ), electrical conductivity (σ) and Seebeck coefficient (S) for a 62-nm-thick Bi_2Te_3 nanoribbon for ion irradiation doses ranging from 0 to 7.5×10^{17} ions/cm² and over the temperature (T) range of 48–373 K. These two-dimensional plots were constructed by interpolating the discrete experimental data points. For completion, the figure of merit ($ZT = S^2\sigma T/\kappa$) is also calculated and shown in Fig. 2(d). A few key effects are seen from these results: (a) Although κ behaves normal as a function of T , the irradiation surprisingly increases κ , from 1.3 W/m-K for the pristine case to a maximum of 1.9 W/m-K for an irradiation dose of 10^{17} ions/cm² at 298 K, and for higher irradiation doses κ is then reduced. (b) σ rises rapidly with the irradiation dose, from 6.77×10^4 S/m for the pristine case to 1.18×10^5 S/m (by a factor of 1.75) for the maximum dose of 7.5×10^{17} ions/cm² at 298 K, and consistently exhibits metallic behavior along the T axis (i.e., decreasing with T). The maximum change in σ occurs at 48 K, increasing by a factor of 2.3. (c) S is also increased by irradiation, although a slight dip is seen at the dose of 10^{17} ions/cm².

To correlate the microstructure of the material with these irradiation effects, we carried out additional TEM and SAED analyses on nanoribbons similarly irradiated as those used in the thermal and electrical measurements, as shown in Fig. 3. The low magnification TEM and SAED images were acquired using a 200 kV JEOL 2100 microscope with a LaB₆ filament and a Gatan Orius charge coupled device (CCD) camera. HRTEM images were captured using a 200 kV FEI monochromated F20 UT Tecnai microscope with optimal high-resolution performance ($C_s = 1.0$ mm) and a 2048×2048 CCD camera positioned after a Gatan Imaging Filter. An electron current density of about 3000 electrons/A²/s for the HRTEM imaging and 15 electrons/A²/s for the low magnification TEM imaging were used. No evidence of electron beam induced sample damage was observed during the imaging. The TEM analysis uncovers that the nanoribbons

retain their single-crystallinity after low-dose ion irradiation ($\leq 10^{17}$ ions/cm²), while amorphous regions gradually develop in the nanoribbons when the dose is higher. This dose threshold for amorphization is in good agreement with experimental results from the literature for 30 keV He⁺ ions incident on silicon and copper.²¹

It is intriguing to compare the irradiation behavior of parameters shown in Fig. 3. Figure 4(a) plots the values of κ , σ , S , and ZT at 300 K normalized by their respective pristine values as a function of irradiation dose. The effective total vacancy concentration simulated using the SRIM program is also shown. It can be seen that the dose of $\sim 10^{17}$ ions/cm² indeed signifies a threshold: beyond this dose, the material is considered to be heavily damaged: σ , S , and ZT begin to rise rapidly, and κ first peaks and then begins to decrease.

The initial rise in thermal conductivity κ upon irradiation is obviously attributed to the increase in electrical conductivity σ , which increases the electronic component of thermal conductivity κ_e as expected from the Wiedemann-Franz law (the phonon component of κ , i.e., κ_{ph} , should not increase upon irradiation, since irradiation will only introduce point defects to scatter phonons). However, subtracting from κ the part of κ_e calculated from the Wiedemann-Franz law using the Sommerfeld value of the Lorenz ratio L_0 , the obtained κ_{ph} is still found to increase upon irradiation. For example, the 300 K value of κ_{ph} then increases from 0.77 W/m-K for the pristine case to 1.27 W/m-K for irradiation with 10^{17} ions/cm², and then starts to drop for higher doses. This is a clear indication that the Lorenz ratio L takes a greater value than L_0 in these nanoribbons, hence the rise in the total κ is due to the rapidly increasing κ_e overpowering the irradiation-suppressed κ_{ph} .

Rather than attempting to accurately determine the value of the Lorenz number L , we estimate the upper and lower bounds of L . Assuming $L = L_0$ for the pristine sample, a lower bound of L for the irradiated samples can be obtained by simply setting κ_{ph} to remain unchanged by irradiation, $\kappa_{ph} = \kappa_{ph}^{\text{pristine}} = \kappa^{\text{pristine}} - L_0\sigma^{\text{pristine}}T$;

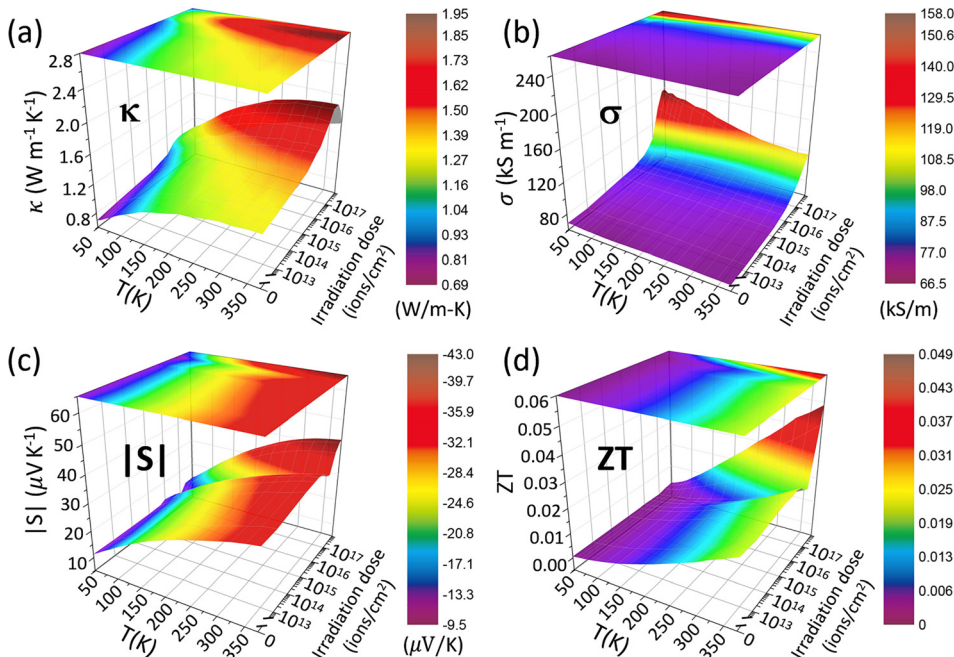


FIG. 2. Thermal and thermoelectric properties of a 62-nm-thick Bi_2Te_3 nanoribbon as functions of temperature (T) and irradiation dose. (a) Thermal conductivity (κ), (b) electrical conductivity (σ), (c) absolute value of the Seebeck coefficient ($|S|$), and (d) figure of merit (ZT).

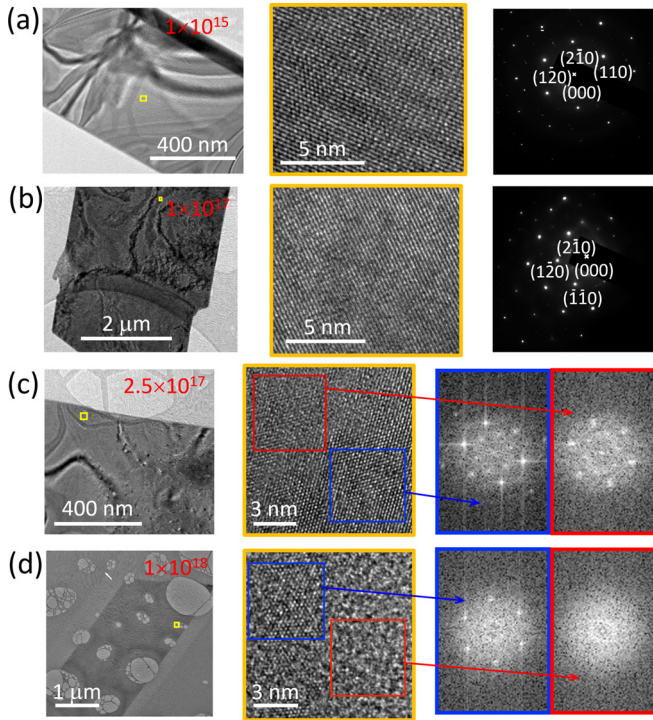


FIG. 3. TEM characterization of Bi_2Te_3 nanoribbons irradiated with different doses. (a) 1.0×10^{15} ions/cm², (b) 1.0×10^{17} ions/cm², (c) 2.5×10^{17} ions/cm², and (d) 1.0×10^{18} ions/cm². (Left column) Low magnification TEM images. (Center column) HRTEM images of the corresponding boxed regions in the low magnification TEM images. (Right column) (a) and (b) SAED patterns (zone axis [001]) for the corresponding HRTEM images, (c) and (d) FFT patterns for boxed regions in the corresponding HRTEM images showing transition from the crystalline to an amorphous state.

hence, $\kappa_e = (\kappa - \kappa^{\text{pristine}}) + L_0 \sigma^{\text{pristine}} T$ and $L_{\text{min}} = (\kappa - \kappa^{\text{pristine}}) / \sigma T + L_0 \sigma^{\text{pristine}} / \sigma$. This treatment gives L_{min} as a function of temperature and irradiation dose, as shown in Fig. 4(b). The fact that this L_{min} still exceeds L_0 for the irradiated samples presents unambiguous evidence that the Wiedemann-Franz law with $L = L_0$ is violated in these materials. A conservative upper bound of L is obtained by setting $\kappa_{\text{ph}} = 0$ at all times, hence $\kappa_e = \kappa$, and $L_{\text{max}} = \kappa / \sigma T$. These upper and lower bounds of L are plotted together in Fig. 4(b) as functions of temperature and irradiation dose.

More importantly, Fig. 4 shows a general trend in which L decreases with temperature and increases with irradiation dose, until the dose exceeds the amorphization threshold (10^{17} ions/cm²). It has been established that ion irradiation of Bi_2Te_3 creates donor-like point defects,¹⁸ leading to an increase in free electron density, hence driving the system into the condition of heavily degenerate doping. Therefore, irradiation continuously displaces the Fermi level (E_F) away from the bandgap into the conduction band. The Fermi level as a function of irradiation has been previously quantified using the concept of displacement damage (D_d). D_d is given by the product of nonionizing energy loss (NIEL) and the irradiating ion fluence, where NIEL is the energy loss responsible for the production of displaced atoms thus creating point defects in semiconductors. Radiation induced effects for different types of radiation (different ion species and energies) are thus

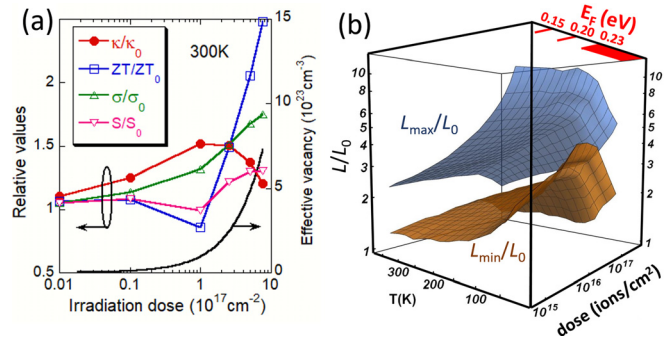


FIG. 4. (a) Relative change for 300 K values of total thermal conductivity (κ), figure of merit ZT, electrical conductivity (σ) and Seebeck coefficient (S) as a function of irradiation dose, normalized by their respective pristine values. Also shown is the SRIM-simulated effective concentration of donor-like vacancies created by irradiation (black line). This number usually overestimates the real defect density as it does not consider self-annealing during irradiation; nevertheless, the curve shows a rapid increase in vacancy concentration with irradiation dose. (b) Experimentally determined upper (L_{max}/L_0) and lower (L_{min}/L_0) bounds of the Lorenz ratio L/L_0 as functions of temperature and irradiation dose and the Fermi level (E_F) position. The base plane is $L = L_0$, the Sommerfeld value of L . The axis of E_F is nonlinear with irradiation dose, and at higher doses E_F is saturated at ~ 0.23 eV, as the electron density can no longer increase.

correlated based on NIEL.¹⁹ NIEL values can be extracted from Monte Carlo SRIM simulation, and we calculate D_d to be up to 2.87×10^{18} MeV/g for doses up to 7.5×10^{17} ions/cm² under the present irradiation condition. Based on the known relationship between E_F and D_d in Bi_2Te_3 ,¹⁸ we can also convert the irradiation dose axis into E_F ; this is also shown in Fig. 4(b). We observe that E_F moves deep into the conduction band for increasing irradiation doses.

It can be concluded that L is constantly higher than L_0 , especially for low temperatures and high E_F values. For narrow-bandgap semiconductors such as Bi_2Te_3 , both low temperature and high E_F are in opposition to the bipolar conduction condition. In fact, using the law of mass action and known effective masses,²² it can be approximately estimated that at room temperature, the electron density is higher than the hole density by over two orders of magnitude ($n = 2 \times 10^{19}$ cm⁻³ and $p = 5 \times 10^{16}$ cm⁻³) for the pristine condition, and increases to over seven orders of magnitude ($n = 6 \times 10^{20}$ cm⁻³ and $p = 2 \times 10^{13}$ cm⁻³) for the irradiation dose of 10^{16} ions/cm². At lower temperatures, the ratio of n/p is expected to be even higher. The fact that σ decreases with temperature [Fig. 2(b)] is also an indication that these materials are degenerately doped with E_F displaced deeply into the conduction band. We note that the conclusion of $L > L_0$ in the unipolar condition is independent of the L value for the pristine sample. We have calculated that (not shown here) regardless of the L value assumed for the pristine sample ($>$, $=$, or $< L_0$), L_{min} of the irradiated sample would grow to $> L_0$ at high doses of irradiation.

The discovery of $L > L_0$ in the heavily unipolar condition can neither be explained by the theory of bipolar transport, nor by the theory of hydrodynamic transport. We tentatively attribute this to the effect of incoherent transport in a metallic system where the conducting electrons no longer behave as long-lived quasi-particles.²³ Assuming the existence of quasi-particles, the mean free path (l) of free electrons in the system could be estimated using the Drude model as $l = \hbar k_F \sigma / ne^2$, where $k_F = (3\pi^2 n)^{1/3}$ is the Fermi wavevector, n is the electron density, and e is the electron charge. The Fermi wavelength (λ_F) is related to the

electron density as $\lambda_F = 2\pi/k_F = 2\pi/(3\pi^2n)^{1/3}$. Using this model, λ_F of these electrons is estimated to be between 8 nm (pristine case) and 2.4 nm (heavily irradiated case), while the mean free path of quasi-particles is in the range from 13 nm (pristine) to 3 nm (heavily irradiated). Therefore, l is close and comparable to λ_F . Hence, the quasi-particles, if exist, would need to be scattered once within a travel distance on the order of their wavelength, a scenario violating the Heisenberg uncertainty principle. In other words, this metallic system is a “bad metal” since it is beyond the Mott-Ioffe-Regel conductivity limit.²⁴ The other independent evidence of the absence of quasi-particles is the high value of the dimensionless figure of merit, $S^2/L \sim 0.02$, much higher than $\sim 10^{-4}$ for typical metals such as Cu and Al. The high S^2/L value for a metal is indicative of non-quasi-particle physics, because otherwise, the small factor $k_B T/E_F$ which usually suppresses inter-particle interactions in a Fermi liquid would equally suppress S , leading to the expectation of very low values of S^2/L . The Wiedemann-Franz law with $L = L_0$ is a direct consequence of quasi-particle transport within the relaxation time limit. Without long-lived quasi-particles, charge and heat are instead transported in the system through independent diffusion modes.²³ Hence, the Lorenz ratio of their conductivities L has no reason to take the value L_0 , and in principle can take any values higher or lower than L_0 , as observed in or proposed for strongly correlated electron materials such as cuprates²⁵ and vanadium dioxide.¹¹ However, if this is the case, detailed mechanisms leading to the absence of quasi-particles in Bi_2Te_3 and the resultant dependence on temperature, doping and irradiation warrants further investigation.

In summary, we discover that the electronic and thermal conductivities in Bi_2Te_3 nanoribbons are unusually high compared to what is expected from a classical transport system, violating the Wiedemann-Franz law. More importantly, this is observed in a regime where the system is degenerately doped with free electrons, which is far from the bipolar conduction condition as previously reported. The observation rules out existing models invoking bipolar conduction or hydrodynamic transport theory, and is tentatively attributed to non-quasi-particle transport in a strongly correlated metallic system.

This work was supported by the U.S. NSF Grant No. DMR-1608899. J.W. acknowledges support from the Tsinghua-Berkeley Shenzhen Institute (TBSI). The materials preparation was supported by Creative Materials Discovery Program through the National Research Foundation of Korea (NRF) funded by the Ministry of Science and ICT (2018M3D1A1058536). H.Z. thanks the support of the U.S. Department of Energy, Office of Science, Office of Basic Energy Sciences, Materials Sciences and Engineering Division, under Contract No. DE-AC02-05CH11231 within the KC22ZH program. The helium ion irradiation experiments were performed at the Biomolecular Nanotechnology Center of the California Institute for Quantitative Biosciences, UC Berkeley. Work at the Molecular Foundry was supported by the Office of Science, Office of Basic Energy Sciences, of the U.S. Department of Energy under Contract No. DE-AC02-05CH11231.

REFERENCES

- M. Thesberg and H. Kosina, “On the Lorenz number of multiband materials,” *Phys. Rev. B* **95**, 125206 (2017).
- X. Wang, V. Askarpour, J. Maassen, and M. Lundstrom, “On the calculation of Lorenz numbers for complex thermoelectric materials,” *J. Appl. Phys.* **123**, 055104 (2018).
- Y. Zhang, N. P. Ong, Z. A. Xu, K. Krishana, R. Gagnon, and L. Taillefer, “Determining the Wiedemann-Franz ratio from the thermal hall conductivity: Application to Cu and $\text{YBa}_2\text{Cu}_3\text{O}_{6.95}$,” *Phys. Rev. Lett.* **84**, 2219 (2000).
- N. Doiron-Leyraud, M. Sutherland, S. Y. Li, L. Taillefer, R. Liang, D. A. Bonn, and W. N. Hardy, “Onset of a boson mode at the superconducting critical point of underdoped $\text{YBa}_2\text{Cu}_3\text{O}_y$,” *Phys. Rev. Lett.* **97**, 207001 (2006).
- M. A. Tanatar, J. Paglione, C. Petrovic, and L. Taillefer, “Anisotropic violation of the Wiedemann-Franz law at a quantum critical point,” *Science* **316**, 1320 (2007).
- H. Pfau, S. Hartmann, U. Stockert, P. Sun, S. Lausberg, M. Brandt, S. Friedemann, C. Krellner, C. Geibel, S. Wirth, S. Kirchner, E. Abrahams, Q. Si, and F. Steglich, “Thermal and electrical transport across a magnetic quantum critical point,” *Nature* **484**, 493 (2012).
- Y. Machida, K. Tomokuni, K. Izawa, G. Lapertot, G. Knebel, J.-P. Brison, and J. Flouquet, “Verification of the Wiedemann-Franz law in YbRh_2Si_2 in a quantum critical point,” *Phys. Rev. Lett.* **110**, 236402 (2013).
- J. K. Dong, Y. Tokiwa, S. L. Bud'ko, P. C. Canfield, and P. Gegenwart, “Anomalous reduction of the Lorenz ratio at the quantum critical point in YbAgGe ,” *Phys. Rev. Lett.* **110**, 176402 (2013).
- R. W. Hill, C. Proust, L. Taillefer, P. Fournier, and R. L. Greene, “Breakdown of fermi-liquid theory in a copper-oxide superconductor,” *Nature* **414**, 711 (2001).
- J. Crossno, J. K. Shi, K. Wang, X. Liu, A. Harzheim, A. Lucas, S. Sachdev, P. Kim, T. Taniguchi, K. Watanabe, T. A. Ohki, and K. C. Fong, “Observation of the Dirac fluid and the breakdown of the Wiedemann-Franz law in graphene,” *Science* **351**, 1058 (2016).
- S. Lee, K. Hippalgaonkar, F. Yang, J. Hong, C. Ko, J. Suh, K. Liu, K. Wang, J. J. Urban, X. Zhang, C. Dames, S. A. Hartnoll, O. Delaire, and J. Wu, “Anomalous low electronic thermal conductivity in metallic vanadium dioxide,” *Science* **355**, 371 (2017).
- Z. Luo, J. Tian, S. Huang, M. Srinivasan, J. Maassen, Y. P. Chen, and X. Xu, “Large enhancement of thermal conductivity and Lorenz number in topological insulator thin films,” *ACS Nano* **12**, 1120 (2018).
- M. T. Pettes, J. Maassen, I. Jo, M. S. Lundstrom, and L. Shi, “Effects of surface band bending and scattering on thermoelectric transport in suspended bismuth telluride nanoplates,” *Nano Lett.* **13**, 5316 (2013).
- A. Weathers, Z. U. Khan, R. Brooke, D. Evans, M. T. Pettes, J. W. Andreasen, X. Crispin, and L. Shi, “Significant electronic thermal transport in the conducting polymer poly(3,4-ethylenedioxythiophene),” *Adv. Mater.* **27**, 2101 (2015).
- H. Yoshino and K. Murata, “Significant enhancement of electronic thermal conductivity of two-dimensional zero-gap systems by bipolar-diffusion effect,” *J. Phys. Soc. Jpn.* **84**, 24601 (2015).
- A. Principi and G. Vignale, “Violation of the Wiedemann-Franz law in hydrodynamic electron liquids,” *Phys. Rev. Lett.* **115**, 56603 (2015).
- P. Kim, L. Shi, A. Majumdar, and P. L. McEuen, “Thermal transport measurements of individual multiwalled nanotubes,” *Phys. Rev. Lett.* **87**, 215502 (2001).
- J. Suh, K. M. Yu, D. Fu, X. Liu, J. Chee, C.-H. Huang, J. Zhou, F. Yang, J. Fan, D. J. Smith, Y.-H. Zhang, J. K. Furdyna, C. Dames, W. Walukiewicz, and J. Wu, “Simultaneous enhancement of electrical conductivity and thermopower in Bi_2Te_3 by native defects,” *Adv. Mater.* **27**, 3681 (2015).
- J. Suh, D. Fu, X. Liu, J. K. Furdyna, K. M. Yu, W. Walukiewicz, and J. Wu, “Fermi-level stabilization in topological insulators Bi_2Se_3 and Bi_2Te_3 : Origin of the surface electron gas,” *Phys. Rev. B* **89**, 115307 (2014).
- J. F. Ziegler, M. D. Ziegler, and J. P. Biersack, “SRIM: The stopping and range of ions in matter (2010),” *Nucl. Instrum. Methods Phys. Res.* **268**, 1818 (2010).
- R. Livengood, S. Tan, Y. Greenzweig, J. Notte, and S. McVey, “Subsurface damage from helium ions as a function of dose, beam energy and dose rate,” *J. Vac. Sci. Technol.*, **B** **27**, 3244 (2009).
- S. Shigetomi and S. Mori, “Electrical properties of Bi_2Te_3 ,” *J. Phys. Soc. Jpn.* **11**, 915 (1956).
- S. A. Hartnoll, “Theory of universal incoherent metallic transport,” *Nat. Phys.* **11**, 54 (2015).
- O. Gunnarsson, M. Calandra, and J. E. Han, “Colloquium: Saturation of electrical resistivity,” *Rev. Mod. Phys.* **75**, 1085 (2003).
- J. A. N. Bruin, H. Sakai, R. S. Perry, and A. P. Mackenzie, “Similarity of scattering rates in metals showing T-linear resistivity,” *Science* **339**, 804 (2013).